Van Den Broeke, M. S., and H. Alsarraf, 2016: Polarimetric radar observations of dust storms at C- and S-band. *J. Operational Meteor.*, **4** (9), 123–131, doi: http://dx.doi.org/10.15191/nwajom.2016.0409.

Journal of Operational Meteorology
Article

Polarimetric Radar Observations of Dust Storms at C- and S-Band

MATTHEW S. VAN DEN BROEKE
Department of Earth and Atmospheric Sciences, University of Nebraska-Lincoln, Lincoln, Nebraska

HUSSAIN ALSARRAF
Kuwait Meteorological Department, Directorate General of Civil Aviation, Kuwait

(Manuscript received 25 January 2016; review completed 22 April 2016)

ABSTRACT

Wind-lofted particles in dust storms exhibit repeatable polarimetric radar characteristics in one C-band and three S-band datasets, including reflectivity factor (Z_H) <25 dBZ and copolar cross-correlation coefficient (ρ_{hv}) <0.65 (and often <0.50). Differential reflectivity (Z_{DR}) varies substantially in dust storms, with values averaging <0 dB in an Arizona case and +1.5 to +4 dB in two southern Plains cases. C-band Z_{DR} was generally +1 to +3 dB in a Kuwait dust storm, similar to the southern Plains cases. Z_{DR} may exhibit small patches of values <–3 dB, especially when observing at an altitude <0.5 km above radar level. Whereas dusty and non-dusty convective outflow boundaries may have similar Z_H characteristics, non-dusty boundaries may be differentiated by their relatively higher Z_{DR} and ρ_{hv} values.

1. Introduction

Wind-lofted dust and sand are common in much of the world including the southwestern United States and the Arabian Peninsula, where cases described in this paper occurred. Dust may be responsible for many problems, including unhealthy concentrations of airborne particulate matter as measured in Arizona (Raman et al. 2014) and over Saudi Arabia and Kuwait (Draxler et al. 2001). The dust may carry diseases (e.g., Sprigg et al. 2014). In addition, the global dust balance likely has a substantial role in the climate system. While the Sahara is the greatest source of airborne dust globally, nearly 12% is estimated to originate from the Arabian Peninsula (Tanaka and Chiba 2006).

Windborne dust and sand frequently occur over the Arabian Peninsula; during certain times of year, >50% of days have visibility reductions due to dust in this region and adjacent northern Africa (Kutiel and Furman 2003). The region is particularly susceptible to dust storms because of the soil composition and low precipitation during much of the year. The wind lofting this material often originates from convective downbursts (Miller et al. 2008). It also may originate as a response to the background synoptic flow. During summertime, a thermal low frequently develops over southern Iran and the southern Arabian Peninsula in response to intense surface heating. Combined with climatologically higher pressure over the Mediterranean Sea, northwest winds frequently are present across the Arabian Peninsula; these are known as the Shamal winds (e.g., Alsarraf and Van Den Broeke 2015). When strong, they may loft substantial dust. The peak season for strong Shamal winds and resulting dust is typically June and July (Alsarraf and Van Den Broeke 2015). Severe dust and sand storms also may result from mid-latitude cold fronts crossing the Arabian Peninsula.

Dust storms in the southwestern United States frequently originate as plumes rising from local areas of favorable land cover (e.g., Lee et al. 2009) and tend to show seasonality with the regional monsoon circulation (e.g., Higgins and Shi 2000). In Arizona, outflow from convective storms associated with the active phase of the southwestern monsoon often initiates dust storms (Raman et al. 2014). Thunderstorms commonly develop over the mountains and gradually move out into surrounding areas during the mid- and late-afternoon, with convective outflows often raising dust (Vukovic et al. 2014). Microbursts associated with this

Corresponding author address: Matthew Van Den Broeke, 306 Bessey Hall, Lincoln, Nebraska 68588
E-mail: mvandenbroeke2@unl.edu

activity may have considerable fine-scale structure, recently resolved using radar observations (Vasiloff and Howard 2009). Dust storms also occur farther east over the southern High Plains of eastern New Mexico, Texas, and Oklahoma—though more sporadically and more closely associated with inter-annual cycles of wind speed, vegetation condition, and soil moisture (Stout 2001). Massive dust events are historically well-known from this region (e.g., Schubert et al. 2004).

Real-time observations of dust storms are essential to allow appropriate warnings to be issued to the public. Radar observations provide one source of this vital information. If airborne dust and sand are present when using conventional Doppler radar, the identity of responsible scatterers may not be evident. Since polarimetric radar observations are becoming more universal, the ability to distinguish between meteorological and non-meteorological targets is well-developed, especially at S-band (~10-cm wavelength). Key polarimetric variables include differential reflectivity (Z_{DR}) and copolar cross-correlation coefficient (ρ_{hv}). Z_{DR} yields information about scatterer orientation, with values >0 dB indicating scatterers that have a relatively larger horizontal axis (e.g., large raindrops, birds) and values <0 dB indicating scatterers with a relatively larger vertical axis (e.g., vertically oriented ice crystals). The ρ_{hv} variable is a measure of how polarization changes between the transmitted and received waves, with lower values indicating a diversity of scatterer species, phases, and/or orientations. Non-meteorological targets typically are associated with very low ρ_{hv} (e.g., Park et al. 2009).

Polarimetric observations have been used to study precipitation and storm systems in detail (e.g., Zrnić and Ryzhkov 1999), and have been applied to thunderstorm electrification (e.g., Lund et al. 2009; Williams et al. 2015). Non-meteorological applications of polarimetric radar observations have included military chaff (Zrnić and Ryzhkov 2004), sea clutter (e.g., Alku et al. 2015), smoke plumes (Melnikov et al. 2009), and biological scatterers (e.g., Van Den Broeke 2013). While radar observations of dust storms have been presented in the literature (e.g., Williams et al. 2009), *polarimetric* dust storm observations have been relatively sparse. S-band polarimetric dust storm observations have been presented from an Arizona event in which large, consistent regions of strongly negative Z_{DR} were noted (Zhang et al. 2015). Z_{DR} was as low as –5 dB in regions with horizontal reflectivity factor (Z_H) near 10 dBZ. For this dust storm, which was observed to reach an altitude of nearly 3 km, negative Z_{DR} values were attributed to debris elements such as sticks and grass that were oriented vertically in a strong electric field (Zhang et al. 2015)—as has been measured in a Sahelian dust event (Williams et al. 2009). It was hypothesized that such strongly negative values of Z_{DR} may be operationally useful for dust storm monitoring. Similar low Z_{DR} values were noted in X-band (~3-cm wavelength) radar observations of the same event.

Many radars operated by governments and private corporations globally are C-band (~5-cm wavelength). Thus, polarimetric signatures of various scatterer types also are important to understand at C-band. C-band and S-band radar observations differ in a few key ways. Given the shorter C-band wavelength, smaller particles scatter in the Mie regime and the resulting resonant effects lead to returns with different properties. For instance, whereas ρ_{hv} values in pure rain are typically near 0.99 at S-band, they frequently drop to 0.93–0.98 at C-band (e.g., Ryzhkov et al. 2007; Anderson et al. 2011). And even though S-band Z_{DR} is often near 0 dB in hail, it may be much higher (i.e., 4–6 dB) at C-band, especially in small melting hail (e.g., Meischner et al. 1991; Tabary et al. 2009; Anderson et al. 2011; Picca and Ryzhkov 2012). Mie scattering at C-band likely occurs for particles >4.5–5 mm in diameter (Kumjian and Ryzhkov 2008), so many of the particles lofted in dust storms are not susceptible to this effect. However, if sufficiently large scatterers (such as dried plant material) are lofted, Mie effects might occur. Another important effect is the increased attenuation and non-uniform beam filling observed at C-band (e.g., Ryzhkov 2007), effectively reducing observed ρ_{hv} values. Because variance of Z_{DR} and ρ_{hv} are a function of the ρ_{hv} magnitude, C-band data tend to be inherently noisier. Though one benefit may be a larger range of ρ_{hv} values at C-band (Palmer et al. 2011), the reduction in ρ_{hv} also may make it difficult to distinguish meteorological and non-meteorological scatterers in C-band data (Kumjian and Ryzhkov 2008). In summary, the primary expected differences are that Z_{DR} values should be higher and ρ_{hv} values lower in many situations at C-band, compared to S-band.

Relatively little is known about differences between C-band and S-band return in dust storms. Given the importance of these events to aviation, human health (e.g., Sprigg et al. 2014), and air quality (e.g., Draxler et al. 2001; Raman et al. 2014)—along with the growing interest in using modeling approaches to nowcast these events (e.g., Vukovic et al. 2014; Huang et al. 2015)—further understanding of radar signatures within dust storms is warranted. Therefore, here we present the first detailed polarimetric radar observations, at C-band and S-band, of several dust storm events from areas prone to this phenomenon. We describe typical values of the polarimetric variables Z_{DR} and ρ_{hv} within these events, and contrast them with polarimetric signatures along a non-dusty convective outflow boundary.

2. Data and methods

Radar datasets are analyzed from the United States S-band Weather Surveillance Radar-1988 Doppler (WSR-88D) network. The upgrade of this network to dual-polarization capability started in 2011 and was completed in 2013. Three dust storm events are analyzed herein, including:

1) an event in the domain of the Phoenix, Arizona, WSR-88D (KIWA) from 0100 to 0400 UTC 6 July 2011, shortly after this radar had been upgraded to polarimetric capability;
2) an event in the domain of the Cannon Air Force Base, New Mexico, WSR-88D (KFDX) from 0000 to 0200 UTC 12 March 2014; and
3) an event in the domain of the Amarillo, Texas, WSR-88D (KAMA) from 2100 to 2300 UTC 18 March 2014.

The dust storm in each event was relatively close to the radar site during the analysis period, with base-scan altitude in the dust generally ≤1 km above radar level (ARL). Using data at a similar altitude aids the comparison between cases, though error may be introduced because particle type, size, and concentration may differ. Nevertheless, these three events provide a range of typical S-band polarimetric observations in dust storms. Z_{DR} and ρ_{hv} are the primary polarimetric variables analyzed, in conjunction with the traditional Z_H.

A C-band, polarimetric radar dataset was obtained from a large dust storm that swept across the Arabian Peninsula on 20 February 2015. Data were obtained from the Kuwait Doppler radar, and extended from 0919 to 1619 UTC 20 February. Characteristics of the Kuwait radar are included in Table 1.

A scatterer-based calibration procedure was applied to quantify any Z_{DR} bias in the KIWA dataset (Ryzhkov et al. 2005; Picca and Ryzhkov 2012). Scatterers examined should be dry snow aggregates ~1.5 km above the ambient 0°C level in the anvil region of convection, which have polarimetric properties including ρ_{hv} >0.97–0.99 and Z_{DR} averaging 0.1–0.2 dB. When this procedure was applied to the KIWA data, an areal average Z_{DR} value within the anvil region was approximately 0 dB, indicating a negative Z_{DR} bias of approximately 0.15 dB. A similar procedure could not be applied to the KFDX and KAMA data because no convection was present in those datasets. The C-band Kuwait radar achieves Z_{DR} calibration via pointing vertically. Heights noted throughout the paper are ARL.

Table 1. Specifications of the Kuwait radar.

Characteristic	Value
Manufacturer	Selex ES GmbH
Wavelength	0.053 m
Peak transmitted power	250 kW
Transmit pulse length	2 μs
Range gate spacing	600 m
Transmit polarization	Simultaneous H/V
Receiver type	Two, one for each H/V
Pulse repetition time	Staggered; 833/1111 Hz
Antenna 3-dB beamwidth	1°
Antenna gain	43 dB
Antenna vertically pointing	Yes
Pedestal scan rate	9° s^{-1}
Z_H range	–31.5 to 95.5 dBZ
Z_{DR} range	–6 to 10 dB

3. S-band polarimetric observations of dust storms

The first S-band polarimetric radar dataset was collected during a historic dust storm in the Phoenix, Arizona, area during July 2011. A severe drought was ongoing, which had led to dry soil and an abundance of readily lofted dust. Thunderstorms developed south of Phoenix in association with the regional monsoon, generating outflow that moved north down the mountain slopes and into the city. The outflow contained wind gusts to 30 m s^{-1}, with dense windborne dust and debris. In this event, the peak hourly concentration of particulate matter with diameter <10 μm (PM10) reached 2575 μg m^{-3} at a station in southern Phoenix (54 times the mean 2011 value), and the peak hourly concentration of particulate matter with diameter <2.5 μm (PM2.5) reached 997 μg m^{-3} (107 times the mean 2011 value). In the second event—collected by KFDX in eastern New Mexico and the western Texas Panhandle during March 2014—a strong, dry cold front moved south over the region with wind gusts to 27 m s^{-1} [National Weather Service (NWS) 2014a]. Finally, the third event was a dust storm that crossed the Texas Panhandle from north to south a week later. It was similar to the other Texas case as a strong, dry cold front progressed across the region with wind gusts to 25 m s^{-1} [National Aeronautics and Space Administration (NASA) 2014; NWS 2014b]. As in the Arizona event, the two southern Plains cases were associated with moderate to extreme region-wide drought after several years of severe drought, reducing vegetation cover and increasing surface dust availability. Key characteristics of the dust storm events analyzed are included in Table 2.

For each sample volume containing dust storm observations at low altitude (generally ≤1 km ARL) and not obviously degraded by issues such as non-uniform beam filling, the dust storm region was demarcated and mean values of the radar variables were computed in this area at base scan. All areas in these events with Z_H ≥5 dBZ were assumed to be dominated by wind-borne material because (i) satellite and visual observations suggested little to no associated precipitation (e.g., NASA 2014; NWS 2014a, 2014b) and (ii) these events happened only when the surface wind speed was strong. Areal mean Z_H was calculated using pixels with Z_H >5 dBZ. For ρ_{hv}, only pixels between 0.208 (the minimum value recorded by a WSR-88D) and 1.000 were included in the areal average because values outside of this range typically are associated with a low signal-to-noise ratio. Mean values of the radar variables for each event—averaged across all analysis times—are summarized in Table 2. Values of the radar variables differed widely between cases. Some of this variation was related to the altitude of radar observations. This association likely was because of a decrease in the concentration of lofted particles with altitude, and because of decreasing ρ_{hv} quality with distance from the radar (e.g., with altitude).

Areal mean Z_H varied from 7 to 11 dBZ in a dust storm sampled by KAMA, and was as high as 23 dBZ in an intense dust plume observed from KFDX (Fig. 1a). Mean Z_H values from the Arizona dust storm fell between these (Table 2). Maximum Z_H values were ~22 dBZ from KAMA, ~35 dBZ from KIWA, and ~52 dBZ from KFDX. In the KFDX and KAMA events, particles were being quickly advected away from their source region by strong north winds, while in the Arizona case, particle lofting was ongoing. Thus, the events from the southern Plains show an increase in Z_H values among observations taken at lower altitude (Fig. 1a) owing to particle settling, while the KIWA

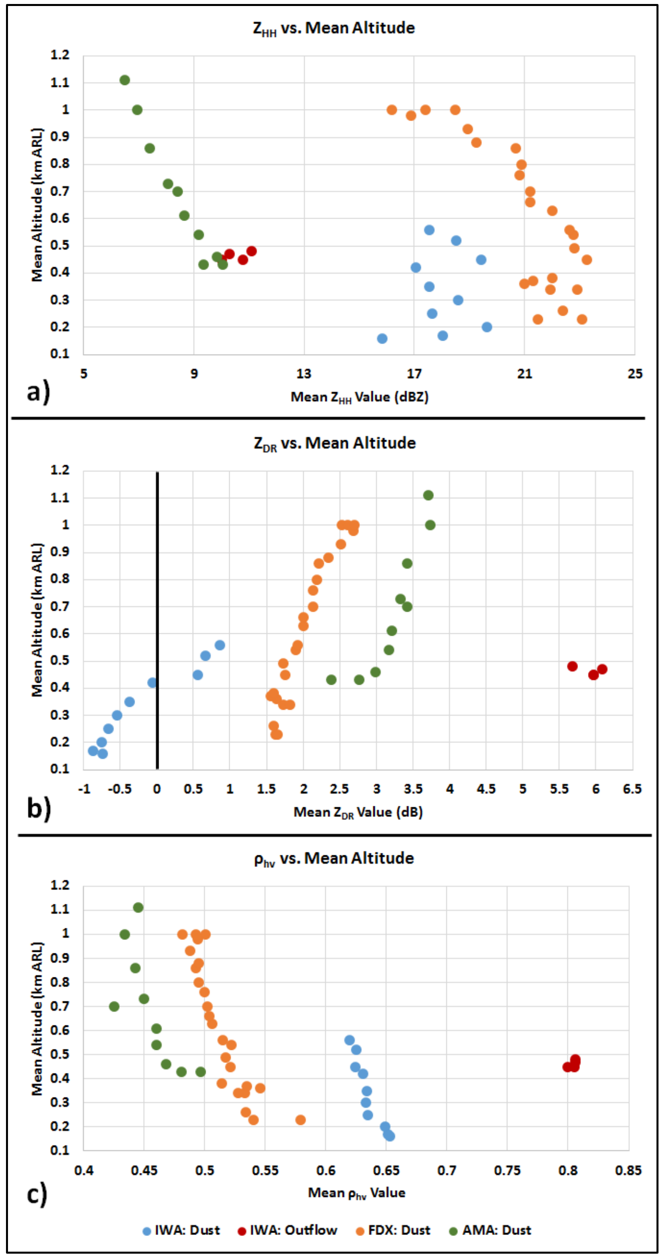

Figure 1. Area-averaged values of (a) Z_H (dBZ), (b) Z_{DR} (dB), and (c) ρ_{hv} from dust storms observed by KIWA (blue dots), KFDX (orange dots), and KAMA (green dots), and for observations along an outflow boundary observed by KIWA (red dots). Values plotted against altitude ARL. *Click image for an external version; this applies to all figures hereafter.*

dust storm did not show a similar altitude dependence. Typical Z_H in a dust event is shown in Fig. 2a.

Z_{DR} values in dust storms varied widely, with areal means not always representative of smaller-scale structure. Areal average Z_{DR} was typically 1.5–4.0 dB in the KFDX and KAMA dust storms (Fig. 1b; Table 2). These values are higher than reported in prior

Table 2. Dates and time ranges over which dust storm observations were analyzed for the four dust storm events, including an outflow boundary observed by KIWA. Also included are mean observation altitudes and mean values of the radar variables, maximum wind speed reported at the surface in the dust or behind the outflow boundary, and radar-derived depth and areal extent for each dust storm event.

Event, Observing Radar	**Dust, KIWA**	**Outflow, KIWA**	**Dust, KFDX**	**Dust, KAMA**	**Dust, Kuwait**
Date of Event	6 July 2011	6 July 2011	12 March 2014	18 March 2014	20 February 2015
Time Range (UTC)	0227–0309	0227–0241	0001–0147	2117–2247	1304–1519
Altitude (km)	0.34	0.46	0.61	0.69	0.94
Z_H (dBZ)	18.0	10.5	20.9	8.4	10–15
Z_{DR} (dB)	–0.2	5.9	2.0	3.2	1.8
ρ_{hv}	0.64	0.80	0.51	0.46	<0.5
Max Wind Speed (m s^{-1})	30	15–16	27	25	20
Max Debris Cloud Depth (km)	3.1	NA	3.8	2.6	4.0
Max Debris Cloud Extent (km^2)	1200	NA	12750	3700	2600

studies (e.g., Zhang et al. 2015), and may indicate a different preferred orientation of debris elements being lofted in this region, or different electrical characteristics in these dust events. A typical example of the Z_{DR} distribution is shown in Fig. 2b. In contrast, areal average Z_{DR} was typically <0 dB in the dust storm observed by KIWA (Fig. 1b), with embedded small areas containing averaged values <–6 dB (e.g., as reported in Zhang et al. 2015). Such patches of remarkably negative Z_{DR} values are seen occasionally in the KAMA and KFDX events, though they are smaller and shorter-lived. In all three events, patches of negative Z_{DR} values at base-scan level were typically seen at altitudes <0.45–0.5 km ARL, with maximum areal extent when observations were at 0.25–0.3 km ARL. Areal average Z_{DR} values typically increased with altitude (Fig. 1b), possibly indicating a reduction in turbulence aloft, which would lessen randomization of horizontally oriented debris elements.

Values of area-averaged ρ_{hv} were consistent with non-meteorological scatterers for all dust events. They ranged from 0.60 to 0.65 in the dust storm observed by KIWA, to generally 0.42–0.55 in the two southern Plains events (Table 2). The ρ_{hv} values were observed to decrease with observation altitude (Fig. 1c). It is unknown why some dust events are characterized by lower mean ρ_{hv} values than others, though the variable type and quantity of lofted particles may be responsible. A typical ρ_{hv} distribution in a dust storm is shown in Fig. 2c.

Dust storms often are associated with propagating boundaries because the wind typically shifts and strengthens behind a boundary. The quantity of material lofted is a strong function of wind speed. Wind-borne particles may concentrate along a boundary, resulting in uncertainty about the source of radar echo. In contrast with the outflow boundary associated with the Phoenix dust storm (observed by KIWA), a non-dusty outflow boundary simultaneously approached Phoenix from the north. Areal mean values of the radar variables were computed along this boundary and compared to observations in the dust storm (Table 2). Values of Z_H were similar between dust and convective outflow boundaries (Fig. 1a; red dots), indicating little discriminating power in this variable. In contrast, Z_{DR} and ρ_{hv} differed markedly between all dust storm observations and the non-dusty outflow boundary (Figs. 1b–c). Z_{DR} was much higher, on average, along the non-dusty boundary, with areal average Z_{DR} generally 5.5–6.0 dB as observed by KIWA (Table 2). Note that a slight *negative* Z_{DR} bias was described for this dataset in the previous section, indicating that these values, though high, are realistic. They are similar to prior Z_{DR} values observed in biological scatterers (Van Den Broeke 2013), which are likely to be a common source of echo along warm-season boundaries (e.g., Achtemeier 1991). The ρ_{hv} values were substantially higher along the non-dusty boundary. Additional cases could help determine if ρ_{hv} can reliably differentiate dusty from non-dusty boundaries.

4. C-band polarimetric observations of a dust storm

A C-band polarimetric radar dataset was available from the 20 February 2015 dust storm that swept across the Arabian Peninsula. In this event, a surface pressure gradient behind a southeastward-propagating cold front led to strong northwest winds and blowing dust and debris across the region. The cold front was associated with a cyclone and strong cold air advection north of the Arabian Peninsula. A time series of hourly meteorological conditions at Kuwait International Airport, near the radar location, is shown in Fig. 3. The

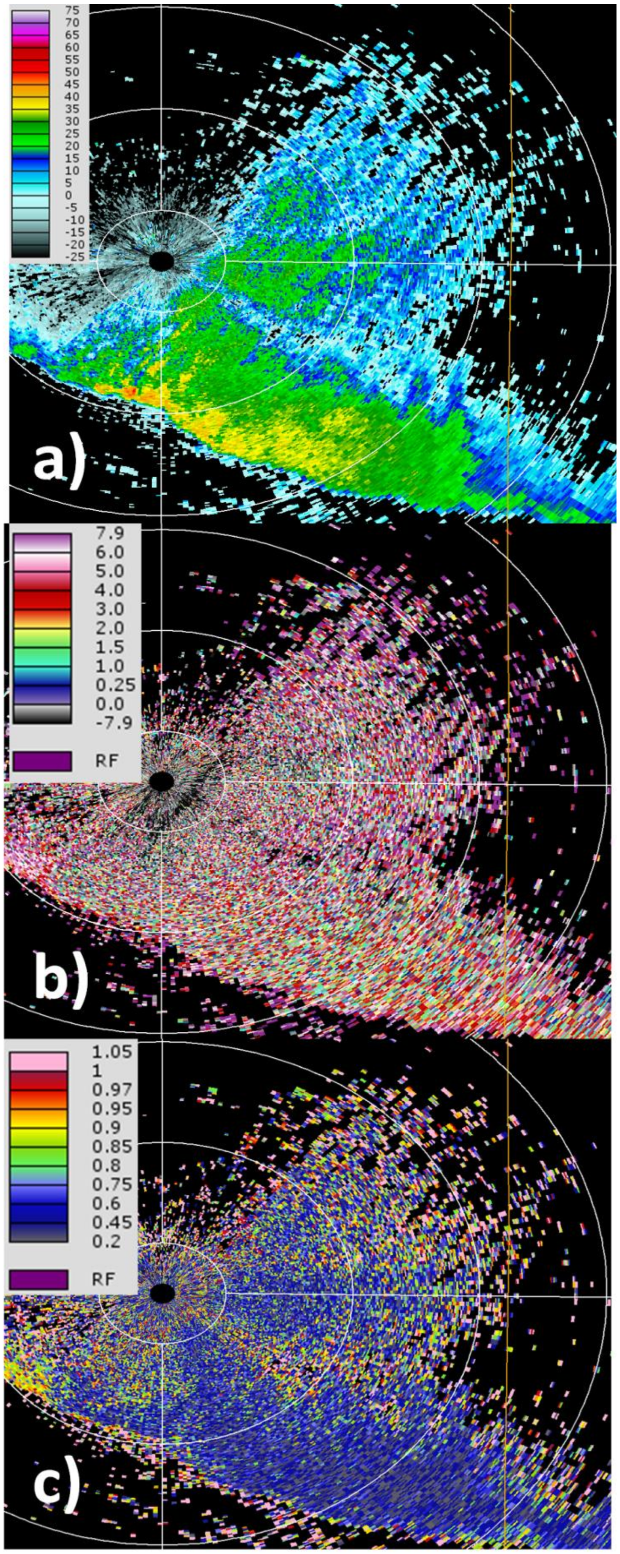

Figure 2. Example dust storm observations from the WSR-88D at Cannon Air Force Base, NM (KFDX), at 0023 UTC 12 March 2014. The elevation angle is 0.54° (i.e., base-scan). (a) is Z_H (dBZ), (b) is Z_{DR} (dB), and (c) is ρ_{hv}. Range rings interval is 20 km, with an innermost range ring at 10 km. Relatively high Z_{DR} and low ρ_{hv} values are indicated in the dust storm, with reflectivity >10 dBZ.

hourly data plotted represent the highest-resolution surface observations available for this site, limiting the ability to show short-timescale weather changes during the dust event. At this airport, a significant meteorological information statement is issued when visibility drops <4.8 km in dust, as recommended by the International Civil Aviation Organization. The Kuwait radar, alongside automated observation stations, are the key tools used to monitor for potential exceedance of this threshold and to determine when hazardous conditions might be approaching.

The analysis period spans from 1319 UTC, when the dust storm became clearly visible to the northwest of the radar, to 1519 UTC, when most of the dust had exited southeastern Kuwait. Maximum Z_H in the dust storm was 20–25 dBZ (e.g., Fig. 4a), generally within 50 km of the radar. Reflectivity was generally greatest near the leading edge of the dust storm, with decreasing Z_H values toward the northwest. Maximum Z_{DR} values in the column contrasted strongly between the dust and pre-dust storm regions. While maximum Z_{DR} averaged 3–7 dB ahead of the dust storm, typical values were only 1–3 dB within the dust (e.g., Fig. 4b). Values ahead of the dust are typical of biological scatterers (Van Den Broeke 2013), which we speculate is the most likely source of these returns given the widespread nature of the signature. These values—because they are typical of what has been observed previously in bioscatter—indicate that any Z_{DR} bias likely is not large enough to affect the results. Lower values within the dust storm are typical, though the presence of relatively high values (>1 dB) may indicate small suspended horizontally oriented scatterers. These relatively high Z_{DR} values also reflect the fact that displayed values are the maximum Z_{DR} in a column, and may reflect the typically higher Z_{DR} values inherent to C-band radars (e.g., Tabary et al. 2009), especially for larger debris elements. Maximum ρ_{hv} values in a column did not distinguish well between biological scatterers and dust storm returns (Fig. 4c), with values always <0.7, and typically <0.5, in each. These values are similar to those expected at S-band, and preclude the possibility of substantial precipitation mixing with the dust in this event. Surface observations across Kuwait indicate no precipitation on this day, except Kuwait International Airport reported 0.03 mm after the most intense portion of the dust storm had ended (from 1600 to 1700 UTC). These observations indicate that precipitation was not widespread and was not associated with the most intense portion of the dust storm.

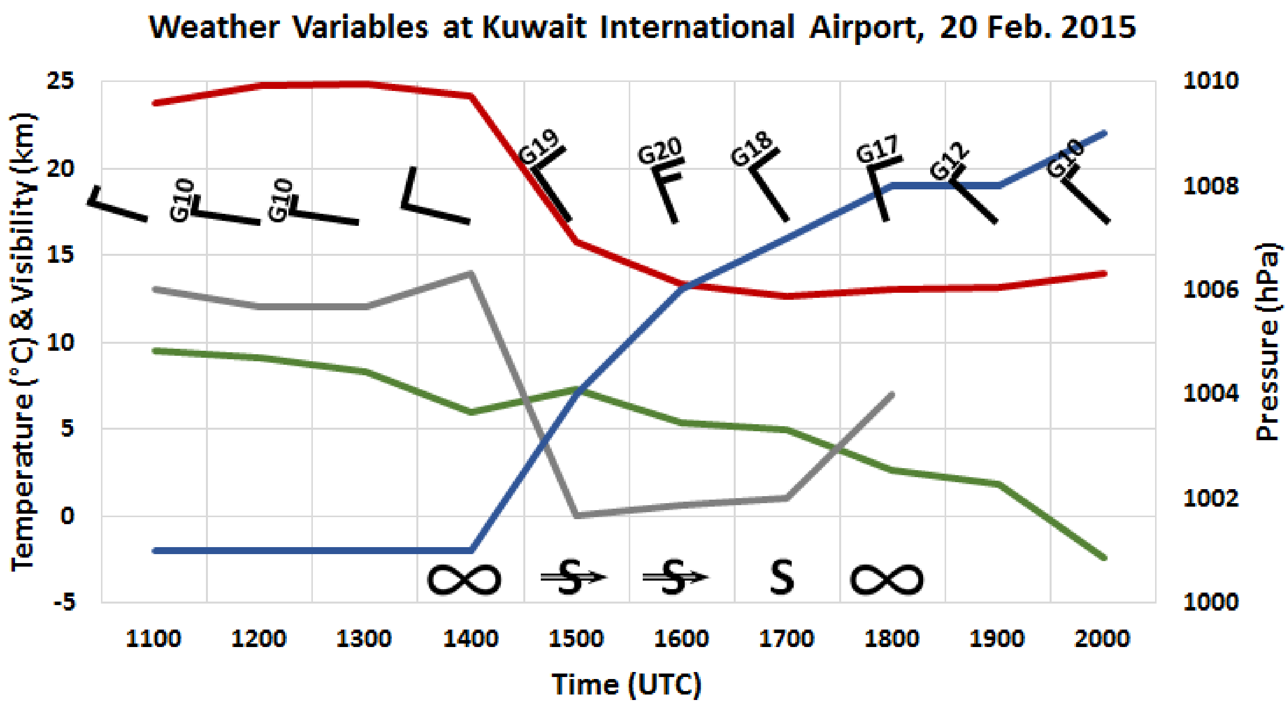

Figure 3. Kuwait International Airport observations from 20 February 2015. The left vertical axis includes temperature (°C; solid red line), dewpoint (°C; solid green line), and visibility (km; solid gray line); and the right vertical axis includes pressure (hPa; solid blue line). Wind observations for each hour are represented by wind barbs (full barb = 10 m s^{-1}; half barb = 5 m s^{-1}), with strong gusts also reported at the end of wind barbs (m s^{-1}). Significant ongoing weather is shown as symbols at the bottom of the chart (following standard conventions).

5. Summary and discussion

Dust storm returns exhibited a high degree of polarimetric variability among the events analyzed herein—while remaining readily distinguishable from a non-dusty boundary. Z_H values typically averaged 10–25 dBZ within dust storms, though higher values are possible in concentrated particle plumes and lower values may occur if particles are relatively diffuse and/or settling out. Mean Z_H values typically decreased as the base-scan observation altitude increased. This variable is not a reliable differentiator between dusty and non-dusty boundaries. Mean Z_H values were similar between C-band and S-band observations reported herein (Table 2).

Area-averaged Z_{DR} values were highly variable within these dust storms, ranging from near –1 dB to near 4 dB (Table 2). Dust storms occasionally include smaller-scale patches with negative Z_{DR} values, possibly indicating a locally strong electric field or a source of debris that can orient vertically. These patches are most commonly observed when the base scan is <0.5 km ARL and typically do not extend through a large portion of the dust storm. Values of Z_{DR} within bioscatter typically average 2–4 dB higher than seen even in the high-Z_{DR} dust events presented here, and thus Z_{DR} is a useful variable for distinguishing dusty from non-dusty boundaries. Values of Z_{DR} within the dust storms were consistent between the C-band dataset and the two S-band datasets from the southern Plains.

Repeatedly across all cases examined here, mean values of ρ_{hv} were consistently low in dust storms (Table 2). S-band observations appeared to differentiate more clearly between biological scatterers and scatterers in dust storms than C-band observations. At S-band, this variable may be useful for distinguishing between dusty and non-dusty boundaries. Observed mean ρ_{hv} tends to decrease with the altitude of base-scan observations. Some of this effect likely is caused by beam broadening with distance from the radar because larger sample volumes inherently have lower ρ_{hv} values. A possible target of future research could be greater understanding of why some dust events have much lower ρ_{hv} values than others. Overall, these observations indicate that polarimetric returns from dust storms are similar at C-band and S-band, and can be used in a nowcasting setting to monitor ongoing

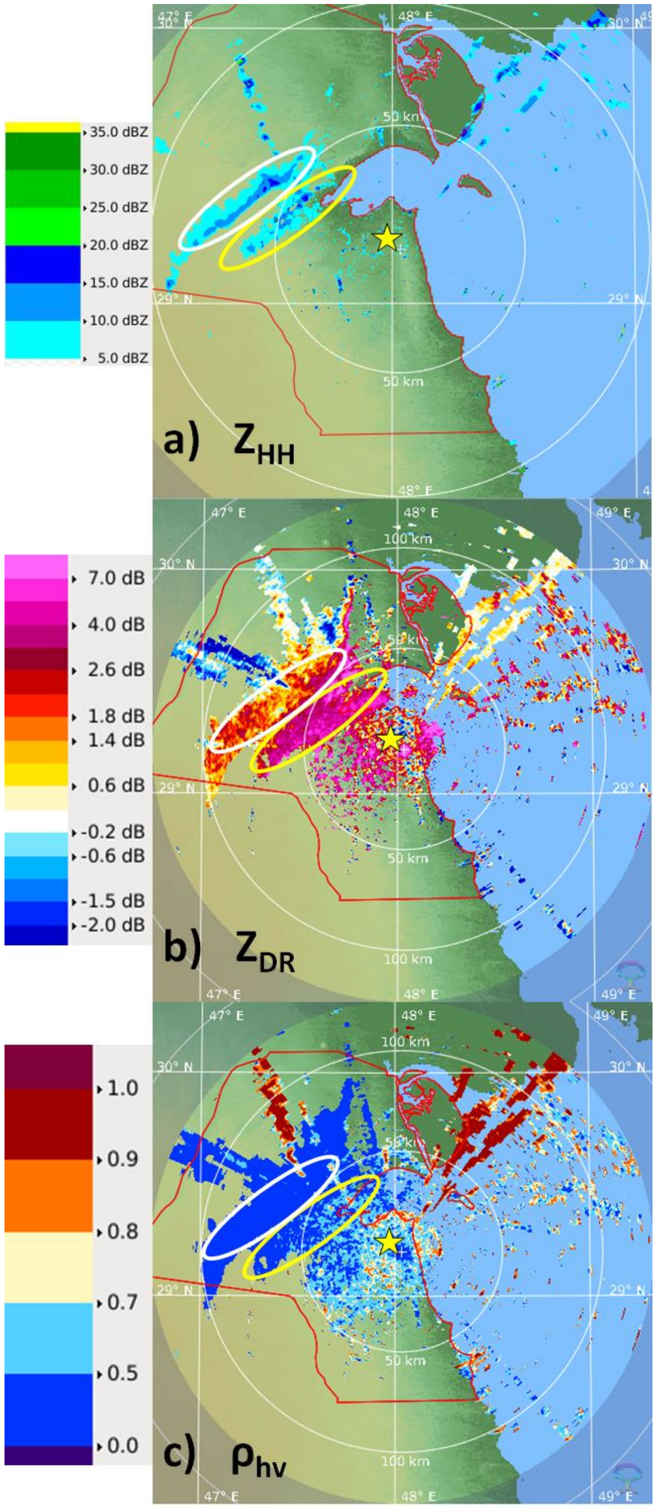

Figure 4. Kuwait (C-band) example of dust storm observations at 1319 UTC 20 February 2015. Variables as labeled in panels. White ellipse indicates dust storm; yellow ellipse indicates area of likely biological scatterers; and yellow star is location of Kuwait International Airport (observations presented in Fig. 3). Spikes extending down-radial to the northwest and northeast likely are clutter.

dust events and to provide notification of possible approaching conditions that are hazardous for aviation.

Acknowledgments. The lead author is supported by an academic appointment at the University of Nebraska-Lincoln. Earle Williams and two anonymous reviewers are thanked for their helpful suggestions that improved the manuscript.

REFERENCES

Achtemeier, G. L., 1991: The use of insects as tracers for “clear-air” boundary-layer studies by Doppler radar. *J. Atmos. Oceanic Technol.*, **8**, 746–765, Crossref.

Alku, L., D. Moisseev, T. Aittomäki, and V. Chandrasekar, 2015: Identification and suppression of nonmeteorological echoes using spectral polarimetric processing. *IEEE Trans. Geosci. Remote Sens.*, **53**, 3628–3638, Crossref.

Alsarraf, H., and M. Van Den Broeke, 2015: Using high-resolution WRF model simulations to investigate the relationship between mesoscale circulations and aerosol transport over Kuwait. *J. Climatol. Wea. Forecasting*, **3** (126), 1–16, Crossref.

Anderson, M. E., L. D. Carey, W. A. Petersen, and K. R. Knupp, 2011: C-band dual-polarimetric radar signatures of hail. *Electronic J. Operational Meteor.*, **12** (2), 1–30. [Available online at www.nwas.org/ej/pdf/2011-EJ2.pdf.]

Draxler, R. R., D. Gillette, J. Kirkpatrick, and J. Heller, 2001: Estimating PM_{10} concentrations from dust storms in Iraq, Kuwait, and Saudi Arabia. *Atmos. Environ.*, **35**, 4315–4330, Crossref.

Higgins, R. W., and W. Shi, 2000: Dominant factors responsible for interannual variability of the summer monsoon in the southwestern United States. *J. Climate*, **13**, 759–776, Crossref.

Huang, M., and Coauthors, 2015: Toward enhanced capability for detecting and predicting dust events in the western United States: The Arizona case study. *Atmos. Chem. Phys.*, **15**, 12595–12610, Crossref.

Kumjian, M. R., and A. V. Ryzhkov, 2008: Polarimetric signatures in supercell thunderstorms. *J. Appl. Meteor. Climatol.*, **47**, 1940–1961, Crossref.

Kutiel, H., and H. Furman, 2003: Dust storms in the Middle East: Sources of origin and their temporal characteristics. *Indoor Built Environ.*, **12**, 419–426, Crossref.

Lee, J. A., T. E. Gill, K. R. Mulligan, M. D. Acosta, and A. E. Perez, 2009: Land use/land cover and point sources of the 15 December 2003 dust storm in southwestern North America. *Geomorphology*, **105**, 18–27, Crossref.

Lund, N. R., D. R. MacGorman, T. J. Schuur, M. I. Biggerstaff, and W. D. Rust, 2009: Relationships between lightning location and polarimetric radar signatures in a small mesoscale convective system. *Mon. Wea. Rev.*, **137**, 4151–4170, Crossref.

Meischner, P. F., V. N. Bringi, D. Heimann, and H. Höller, 1991: A squall line in southern Germany: Kinematics and precipitation formation as deduced by advanced polarimetric and Doppler radar measurements. *Mon. Wea. Rev.*, **119**, 678–701, Crossref.

Melnikov, V. M., D. S. Zrnić, and R. M. Rabin, 2009: Polarimetric radar properties of smoke plumes: A model. *J. Geophys. Res.*, **114**, D21204, Crossref.

Miller, S. D., A. P. Kuciauskas, M. Liu, Q. Ji, J. S. Reid, D. W. Breed, A. L. Walker, and A. A. Mandoos, 2008: Haboob dust storms of the southern Arabian Peninsula. *J. Geophys. Res.*, **113**, D01202, Crossref.

NASA, cited 2014: Dust storm blows across Texas. [Available online at earthobservatory.nasa.gov/IOTD/view.php?id=83375.]

NWS, cited 2014a: Two rounds of wind and dust: 11 March 2014. [Available online at www.srh.noaa.gov/lub/?n=events-2014-20140311-wind.]

____, cited 2014b: Another day of wind and dust: 18 March 2014. [Available online at www.srh.noaa.gov/lub/?n=events-2014-20140318-wind.]

Palmer, R. D., and Coauthors, 2011: Observations of the 10 May 2010 tornado outbreak with OU-PRIME: Potential for new science with high-resolution polarimetric radar. *Bull. Amer. Meteor. Soc.*, **92**, 871–891, Crossref.

Park, H.-S., A. V. Ryzhkov, D. S. Zrnić, and K.-E. Kim, 2009: The hydrometeor classification algorithm for the polarimetric WSR-88D: Description and application to an MCS. *Wea. Forecasting*, **24**, 730–748, Crossref.

Picca, J., and A. Ryzhkov, 2012: A dual-wavelength polarimetric analysis of the 16 May 2010 Oklahoma City extreme hailstorm. *Mon. Wea. Rev.*, **140**, 1385–1403, Crossref.

Raman, A., A. F. Arellano Jr., and J. J. Brost, 2014: Revisiting haboobs in the southwestern United States: An observational case study of the 5 July 2011 Phoenix dust storm. *Atmos. Environ.*, **89**, 179–188, Crossref.

Ryzhkov, A. V., 2007: The impact of beam broadening on the quality of radar polarimetric data. *J. Atmos. Oceanic Technol.*, **24**, 729–744, Crossref.

____, S. E. Giangrande, V. M. Melnikov, and T. J. Schuur, 2005: Calibration issues of dual-polarization radar measurements. *J. Atmos. Oceanic Technol.*, **22**, 1138–1155, Crossref.

____, and Coauthors, 2007: Comparison of polarimetric algorithms for hydrometeor classification at S and C bands. Preprints, *33rd Conference on Radar Meteorology*, Cairns, Queensland, Australia, Amer. Meteor. Soc., 10.3. [Available online at ams.confex.com/ams/pdfpapers/123109.pdf.]

Schubert, S. D., M. J. Suarez, P. J. Pegion, R. D. Koster, and J. T. Bacmeister, 2004: On the cause of the 1930s Dust Bowl. *Science*, **303**, 1855–1859, Crossref.

Sprigg, W. A., and Coauthors, 2014: Regional dust storm modeling for health services: The case of valley fever. *Aeolian Res.*, **14**, 53–73, Crossref.

Stout, J. E., 2001: Dust and environment in the southern High Plains of North America. *J. Arid. Environ.*, **47**, 425–441, Crossref.

Tabary, P., F. Vulpiani, J. J. Gourley, A. J. Illingworth, R. J. Thompson, and O. Bousquet, 2009: Unusually high differential attenuation at C-band: Results from a two-year analysis of the French Trappes polarimetric radar data. *J. Appl. Meteor. Climatol.*, **48**, 2037–2053, Crossref.

Tanaka, T. Y., and M. Chiba, 2006: A numerical study of the contributions of dust source regions to the global dust budget. *Glob. Planet. Change*, **52**, 88–104, Crossref.

Vasiloff, S. V., and K. W. Howard, 2009: Investigation of a severe downburst storm near Phoenix, Arizona, as seen by a mobile Doppler radar and the KIWA WSR-88D. *Wea. Forecasting*, **24**, 856–867, Crossref.

Van Den Broeke, M. S., 2013: Polarimetric radar observations of biological scatterers in Hurricanes Irene (2011) and Sandy (2012). *J. Atmos. Oceanic Technol.*, **30**, 2754–2767, Crossref.

Vukovic, A., and Coauthors, 2014: Numerical simulation of "an American haboob." *Atmos. Chem. Phys.*, **14**, 3211–3230, Crossref.

Williams, E., N. Nathou, E. Hicks, C. Pontikis, B. Russell, M. Miller, and M. J. Bartholomew, 2009: The electrification of dust-lofting gust fronts ('haboobs') in the Sahel. *Atmos. Res.*, **91**, 292–298, Crossref.

____, and Coauthors, 2015: Measurements of differential reflectivity in snowstorms and warm season stratiform systems. *J. Appl. Meteor. Climatol.*, **54**, 573–595, Crossref.

Zhang, P., D. Zrnić, and A. Ryzhkov, 2015: Observations of negative Z_{DR} in sandstorms. Preprints, *37th Conference on Radar Meteorology*, Norman, OK, Amer. Meteor. Soc, 259. [Available online at ams.confex.com/ams/37RADAR/webprogram/Handout/Paper275678/37thPoster_PZhang.pdf.]

Zrnić, D. S., and A. V. Ryzhkov, 1999: Polarimetry for weather surveillance radars. *Bull. Amer. Meteor. Soc.*, **80**, 389–406, Crossref.

____, and ____, 2004: Polarimetric properties of chaff. *J. Atmos. Oceanic Technol.*, **21**, 1017–1024, Crossref.